1992

Experimental Dual-mode Control of a Flexible Robotic Arm

Woosoon Yim
University of Nevada, Las Vegas, woosoon.yim@unlv.edu

Jichun Zuang
University of Nevada, Las Vegas

Sahjendra N. Singh
University of Nevada, Las Vegas, sajendra.singh@unlv.edu

Robotica (1992) volume 10, pp 135–145

Experimental dual-mode control of a flexible robotic arm

Woosoon Yim, Jichun Zuang and Sahjendra Singh

Department of Mechanical Engineering, University of Nevada, Las Vegas, 4505 Maryland Parkway, Las Vegas, Nevada 89154 (USA)

(Received in Final Form: May 17, 1991)

SUMMARY

This paper focuses on the implementation of a dual-mode controller for the maneuver of a single link flexible robotic arm. The joint angle trajectory tracking is accomplished by a proportional and derivative PD and a feedforward controller. Based on the pole placement technique, a linear stabilizer is designed for elastic mode stabilization. The stabilizer is switched on when the trajectory reaches the vicinity of the terminal state, and the effect of switching time on arm vibration is investigated. An optical deflection sensor is used for on-line measurements of elastic deflections, and also used for the prediction of the static deflection of the arm in the target position. The robustness of the linear stabilizer at varying payloads is presented.

KEYWORDS: Flexible arm; Dual-mode controller; Trajectory tracking; Static deflection.

1. INTRODUCTION

Light weight robotic arms have many advantages over bulky, rigid ones: higher speed of operation, less energy consumption, smaller actuator size, to name a few. However, a light weight arm also makes its controller much more complicated than that of a rigid one because of its inherent structural flexibility.

Since the early 70's, efforts have been made in this area of dynamics and control of elastic robotic systems. The dynamic modeling of a robot with elastic link has been investigated by many researchers.[1–3] Equally important are the various control schemes proposed using adaptive, self-tuning, and inversion techniques.[4–8] While much has been done in the analytical field, relatively little has been done in the laboratory.

We present in this paper a control system design for the control of a single link elastic robotic arm based on a dual-mode control technique and on the results of laboratory experiments. In the dual-mode control approach, the trajectory evolves in two phases: In the first phase of maneuver, the joint angle is controlled, and in the second phase vibration damping is accomplished.

For a joint angle trajectory control, a PD controller is constructed based on an experimentally identified servomotor model. An input shaping filter is designed in the feedforward loop so that a ramp command trajectory can be tracked. Interestingly, the joint angle PD controller does not use elastic mode feedback in contrast to the dual-mode controllers.[7] This is due to the fact that the interacting torque at the joint due to the elastic oscillation of the link is small compared to the torque developed by the PD controller. Using the joint angle controller, the arm can be maneuvered to follow a given joint angle trajectory command accurately. However, this excites the elastic modes, and it becomes necessary to damp the elastic motion.

The advantage of using the joint angle controller is that when the joint angle reaches the vicinity of the terminal state, the only significant motion remaining in the system is due to elastic vibration. Thus in the terminal phase, the system is well represented by a linear model, since in the robotic arm model only significant nonlinearity is due to the rigid mode. Based on an asymptotically linearized model, a stabilizer is designed using a pole placement technique. For the synthesis of the controller, only measured variables are used. The elastic mode is obtained by an optical deflection sensor consisting of a diode laser and a position photodiode. The derivative of the elastic mode feedback is obtained by digitally differentiating the measured deflection signal of link tip position.

The complete closed-loop system is designed in the laboratory and experiments are performed to verify joint angle tracking and vibration stabilization capability to follow various command trajectories. The sensitivity of the controller to payload variations is also examined. The effect of choice of a smooth command trajectory on elastic deflection is examined. Although the stabilizer has been designed for the terminal phase, experimental results indicate that the control system is quite robust, and one can leave the stabilizer loop closed throughout and still obtain a stable response. Selected experimental results are presented to show that precise tracking and elastic mode stabilization are accomplished in the closed-loop system in spite of the payload variation.

The organization of the paper is as follows. Section 2 presents the PD controller and the feedforward filter design. The mathematical model and the stabilizer design are presented in Section 3. A description of experimental setup is given in Section 4, and 5 presents experimental results.

2. EXPERIMENTAL SETUP

As shown in Figure 1, the mechanical assembly consists of a rigid stand, a bracket, and a flexible link with a lumped mass at its tip. A DC servo motor (Inertial Motors Co., model D30-S) with a speed reducer (1:80, Harmonic Drive, model PCR3C) is used for the second joint actuator (Note: the first motor is not used in this

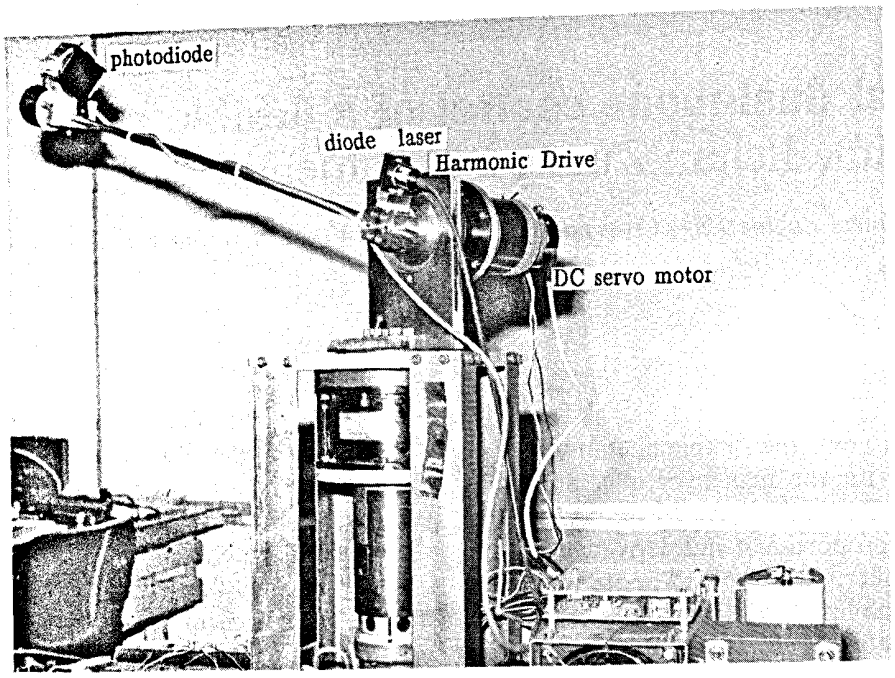

Fig. 1. Experimental setup of a flexible robotic arm.

research). The value of parameters used for a flexible arm is as follows:

lumped mass at link tip (m) = 0.728 kg
link length (l) = 0.609 m
Modulus of elasticity (E) = 2×10^{11} psi
area moment of inertia (I) = 4.26×10^{-10} m^4

An IBM compatible microcomputer with data acquisition system (Burr–Brown PCI-20041 carrier with A/D, D/A, and counter) is used for signal measurement and control. A lateral effect photodiode (UDT LSC30D) with a diode laser generator (780 nm) is used as a link tip deflection sensor[9] as shown in Figure 2, and a bandpass filter is used in front of the photodiode to filter out ambient light. The photodiode is connected to a transimpedance amplifier and calibrated for link tip deflection. An encoder signal is fed to the counter via a decoding circuit and the synchronization of controller is based on the pacer clock (8 MHz) on the carrier.

3. JOINT ANGLE CONTROLLER

The joint angle controller, designed to track the reference joint angle trajectory, consists of a PD controller and an input shaping filter in the feedforward loop. The transfer function of the servomotor is identified experimentally. Based on this transfer function, feedback gains of the controller are obtained.

3.1 Plant modeling

Since the amplifier is designed for the velocity servo controller, the velocity feedback gain k_d is adjusted on the amplifier such that there is no joint velocity overshoot. The transfer function of the system shown in Figure 3 including the velocity feedback loop of gain k_d is experimentally determined by applying a unit step input. Assuming a first order plant, the difference equation of the system becomes,

$$\omega_n = \alpha\omega_{n-1} + \beta v_{n-1} + \varepsilon \tag{1}$$

where α and β are the coefficients to be determined, ε denotes the error signal, ω is the angular velocity, and v is the input signal.

Using the least squares method,[10] the value of the coefficients are found to be $\alpha = 0.9$ and $\beta = 1.65$. Thus equation (1) gives

$$\omega_n = 0.9\omega_{n-1} + 1.65v_{n-1} \tag{2}$$

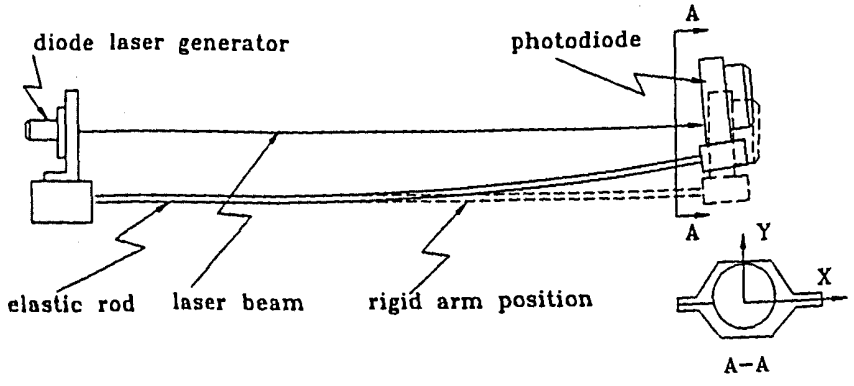

Fig. 2. Optical deflection sensor.

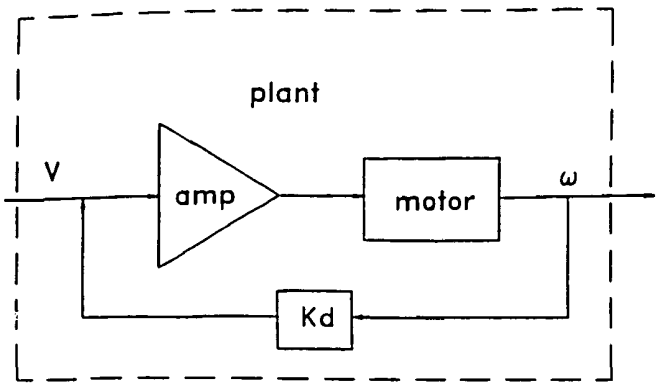

Fig. 3. Joint velocity control loop.

Taking the z-transform of equation (2) gives

$$\frac{\Omega(z)}{V(z)} = G(z) = \frac{1.65z^{-1}}{1-0.9z^{-1}} \tag{3}$$

3.2 PD controller

Figure 4 shows the block diagram of the system with PD controller. Using the relation of $\theta(z)/\Omega(z) = Tz^{-1}/(1-z^{-1})$ with $T = 0.01$ sec and equation (3), the transfer function of Figure 4 becomes,

$$\frac{\theta(z)}{X(z)} = \frac{0.0165k_p z^{-1}}{1-1.9z^{-1}+(0.9+0.0165k_p)z^{-2}} \tag{4}$$

For the stability of the closed-loop system, the value of k_p must satisfy

$$0 \le k_p \le 6.06$$

The value of k_p used in this experiment is 0.8 and the sampling frequency are chosen to be 100 Hz.

An experiment was performed to examine the joint angle tracking ability of the closed-loop system. A command joint angle trajectory was chosen as shown in Figure 5 where the arm moves to the target position and returns to the original position after a specified interval. It was experimentally found that the PD controller designed by the servomotor accomplished the trajectory tracking of the arm. However, a small steady state joint angle tracking error exists as shown in Figure 5. In order to eliminate the tracking error, either an integrator or a feedforward loop must be included in addition to the PD controller. Because of an unacceptable joint angle overshoot with an integrator, a feedforward filter is chosen. The design of the feedforward filter is presented below.

3.3 Feedforward filter

A first order filter of the form $F(z) = f(1-z^{-1})$ is used in the forward path as shown in Figure 6; f is a constant to be determined later. The transfer function including $F(z)$ with k_p of 0.8 is

$$\frac{\theta(z)}{X(z)} = \frac{0.0132z^{-2}(1+F(z))}{(1-0.9z^{-1})(1-z^{-1})+0.0132z^{-2}} \tag{5}$$

and the error transfer function is

$$\frac{E(z)}{X(z)} = \frac{(1-0.9z^{-1})(1-z^{-1})-0.0132z^{-2}F(z)}{(1-0.9z^{-1})(1-z^{-1})+0.0132z^{-2}} \tag{6}$$

The controller will be designed to follow ramp and step commands. We assume that any command trajectory can be obtained by piecing together the ramp and step functions. The filter parameter f is chosen such that the steady state error for a ramp input is zero. For a ramp input $X(z) = Tz^{-1}/(1-z^{-1})^2$, the error equation becomes

$$E(z) = \frac{\{(1-0.9z^{-1})-0.0132z^{-2}f\}Tz^{-1}}{\{(1-0.9z^{-1})(1-z^{-1})+0.0132z^{-2}\}(1-z^{-1})} \tag{7}$$

Using the final value theorem,

$$e_{ss} = \lim_{z\to 1}(1-z^{-1})E(z) = \frac{(0.1-0.0132f)T}{0.0132} \tag{8}$$

From equation (8) e_{ss} becomes zero if and only if $f = 7.6$.

Figure 7 shows the experimental result of the joint angle control. We notice that unlike Figure 5, the steady state error vanishes in the closed-loop system including the feedforward controller.

4. STABILIZER DESIGN

Using the derived controller, including the PD loop and the input shaping filter, one can follow precisely a desirable joint angle command trajectory. However, the maneuver of the arm excites the elastic modes of the link, and it becomes necessary to damp the elastic vibration. For the design of stabilizer it is essential to obtain the mathematical model of the arm.

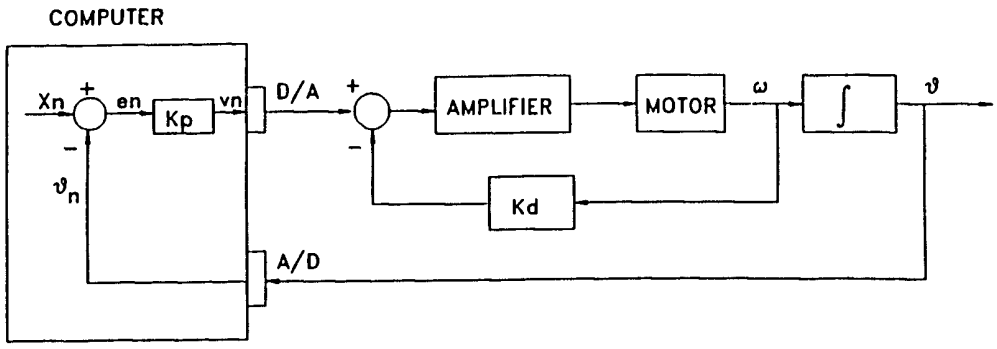

Fig. 4. Joint position control loop.

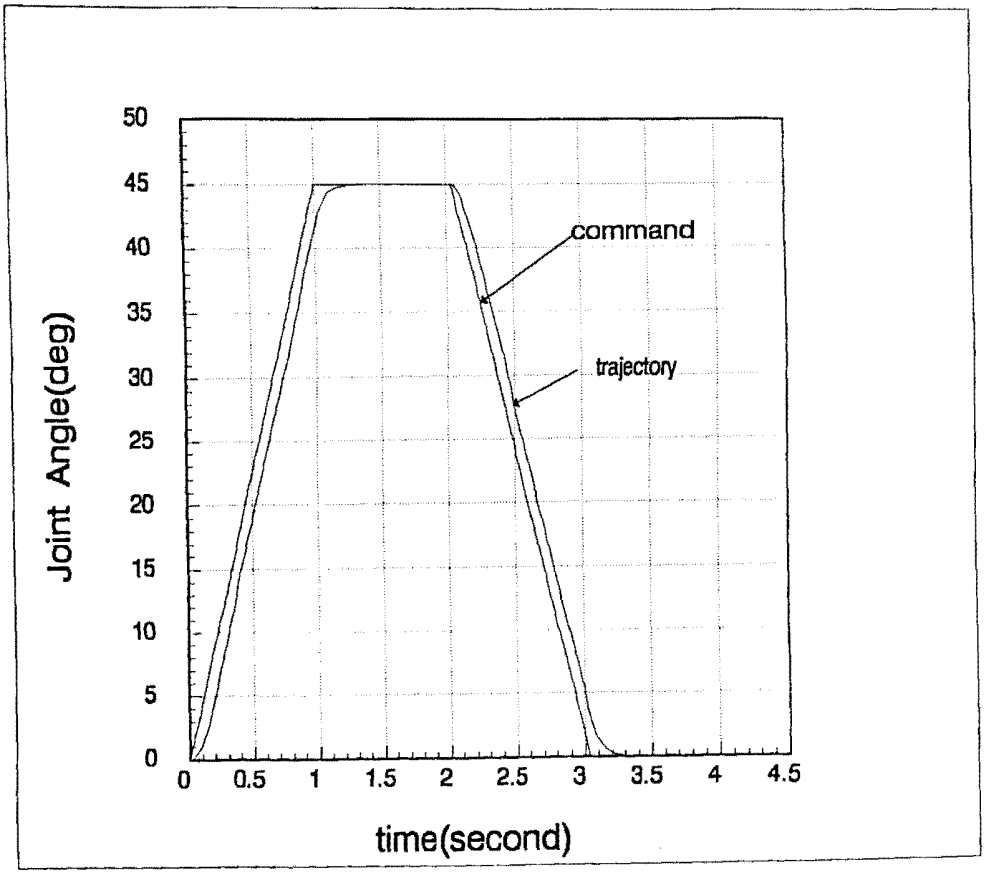

Fig. 5. Joint angle trajectory tracking without feedforward filter.

4.1 Dynamic modeling

Using the assumed-modes method,[1] we can express the link deflection w due to elasticity as follows:

$$w = \sum_{i=1}^{n} \gamma_i q_i \tag{9}$$

where γ_i is the admissible function and q_i is the generalized coordinate. Using the Lagrange's equations, the dynamic equations of a single link shown in Figure 8 becomes

$$\frac{d}{dt}\left(\frac{\partial K}{\partial \dot{\mathbf{p}}}\right) - \frac{\partial K}{\partial \mathbf{p}} + \frac{\partial U}{\partial \mathbf{p}} = \mathbf{Q} \tag{10}$$

where K is the kinetic energy, U is the potential energy, $\mathbf{p} = [\theta, q_1, q_2, \ldots, q_n]^T$, $\mathbf{Q} = [\tau, 0, 0, \ldots, 0]^T$, and τ is the actuator torque.

For simplicity, only one mode of vibration will be considered, i.e. $n = 1$ in equation (9). The admissible functions, γ_i, chosen here are based on the mode shapes of a fixed-free beam with lumped mass at the tip.

Using equation (9) and (10), one can easily derive the following equations:

$$M_1\ddot{\theta} + M_2\ddot{q} + Q_1\dot{q}\dot{\theta} + G_1 = \tau \tag{11}$$

$$M_3\ddot{\theta} + M_4\ddot{q} + Q_2\dot{q}\dot{\theta} + G_2 = 0 \tag{12}$$

where

$$M_1 = \rho q^2 \int_0^l \gamma^2\, dr + m\gamma^2(l)q^2 + \rho l^3/3 + ml^3$$

$$M_2 = \rho \int_0^l \gamma r\, dr + ml\gamma(l)$$

$$M_3 = M_2$$

$$M_4 = \rho \int_0^l \gamma^2\, dr + m\gamma^2(l)$$

$$Q_1 = 2\rho q \int_0^l \gamma^2\, dr + 2m\gamma^2(l)q$$

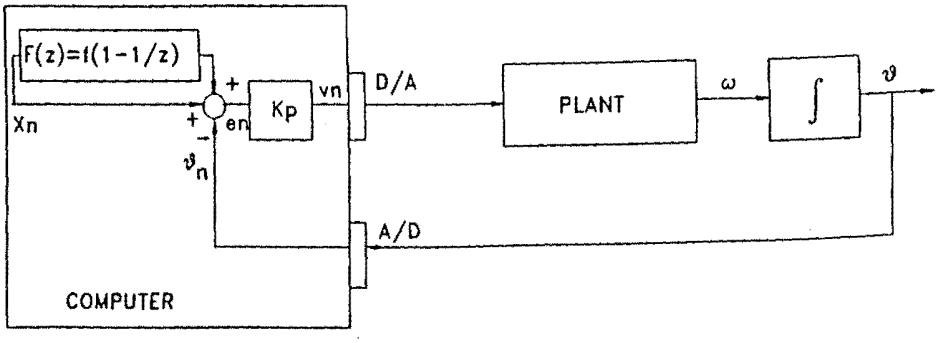

Fig. 6. Joint position control loop with feedforward filter.

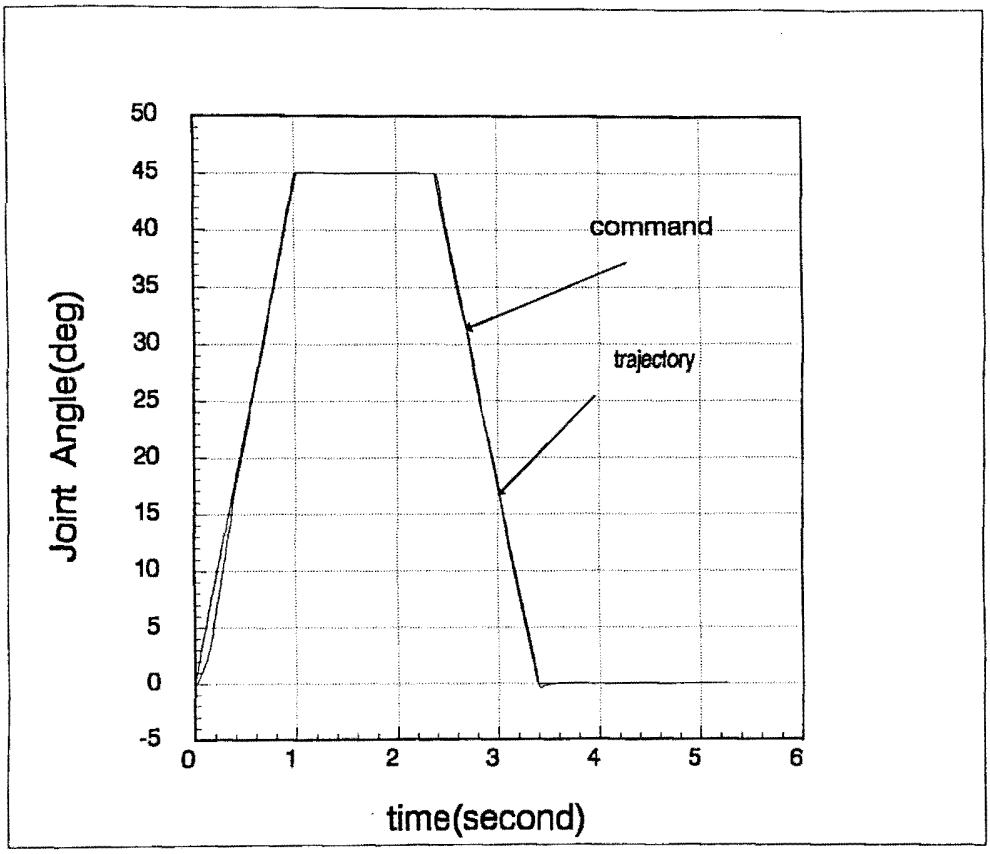

Fig. 7. Joint angle trajectory tracking with feedforward filter.

$$Q_2 = -\rho q \int_0^l \gamma^2\, dr - mq\gamma^2(l)$$

$$G_1 = -mgq\gamma(l)\sin\theta - \rho g q \sin\theta \int_0^l \gamma\, dr + \{\rho g l^2/2 + mgl\}\cos\theta$$

$$G_2 = qEI\int_0^l \gamma''^2\, dr + mg\gamma(l)\cos\theta + \rho g\cos\theta\int_0^l \gamma\, dr$$

ρ = mass per unit length

g = gravity

4.2 Linearization

For an appropriate joint angle command trajectory terminating at $\theta = \theta^*$, we note that in the closed-loop system, including the PD and feedforward controller, $\theta(t) \to \theta^*$ and $\dot{\theta}(t) \to 0$ as $t \to \infty$. As the trajectory of the system enters a small neighborhood of the terminal state ($\theta = \theta^*$, $\dot{\theta} = 0$) after a finite time, the closed-loop system is well approximated by a linear system. Thus, the design of stabilizer based on the asymptotically linearized model is adequate.

Let w^* and θ^* be the static deflection of the arm and the terminal value of the joint angle, respectively. (They

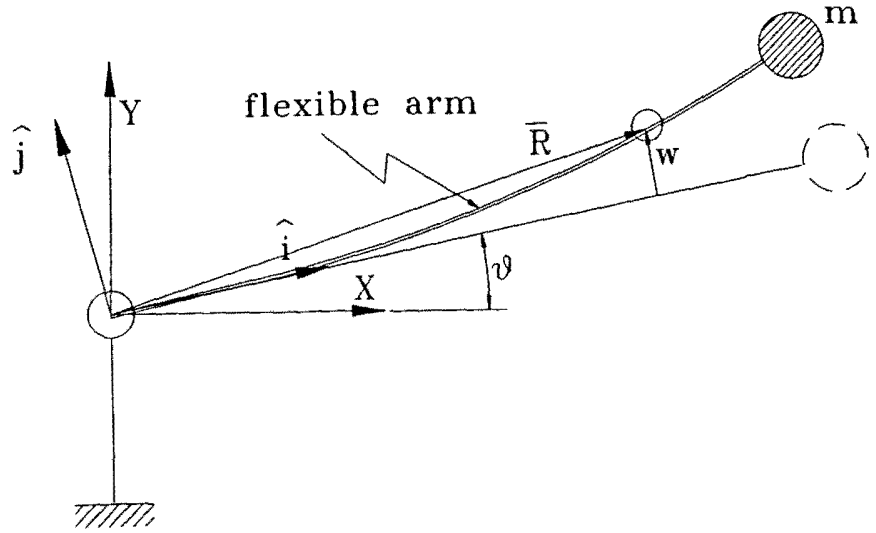

Fig. 8. Model of a single link flexible arm.

constitute the equilibrium point of the system.) Then the actual arm deflection and joint angle around the equilibrium point can be expressed by

$$w = w^* + \Delta w \quad \text{or} \quad q = q^* + \Delta q \tag{13}$$

$$\theta = \theta^* + \Delta\theta \tag{14}$$

where $q^* = w^*/\gamma$ and Δq, $\Delta\theta$ denote the deviation of q and θ from q^* and θ^*. Also,

$$\dot{q} = \Delta\dot{q} \tag{15}$$

$$\dot{\theta} = \Delta\dot{\theta} \tag{16}$$

Using equations (13) to (16), we can expand equations (11) and (12) in the Taylor series at the equilibrium point (θ^*, q^*). Ignoring the second order terms, equations (11) and (12) become

$$M_1^* \Delta\ddot{\theta} + M_2^* \Delta\ddot{q} + R_1(q^*, \theta^*)\Delta q + R_2(q^*, \theta^*)\Delta q = \Delta\tau \tag{17}$$

$$M_3^* \Delta\ddot{\theta} + M_4^* \Delta\ddot{q} + R_3(q^*, \theta^*)\Delta\theta + R_4(q^*, \theta^*)\Delta q = 0 \tag{18}$$

$$M_i^* = M_i(\theta^*, q^*)$$

$$R_1 = \frac{\partial G_1}{\partial\theta} = -\left[\left\{mg\gamma(l) + \rho g\int \gamma\, dr\right\} \times q^* \cos\theta^* + (\rho g l^2/2 + mgl)\sin\theta^*\right]$$

$$R_2 = \frac{\partial G_1}{\partial q} = -\left\{mg\gamma(l) + \rho g\int \gamma\, dr\right\}\sin\theta^*$$

$$R_3 = \frac{\partial G_2}{\partial\theta} = R_2$$

$$R_4 = \frac{\partial G_2}{\partial q} = EI\int \gamma''^2\, dr$$

or in matrix form,

$$\begin{pmatrix} M_1^* & M_2^* \\ M_3^* & M_4^* \end{pmatrix}\begin{Bmatrix} \Delta\ddot{\theta} \\ \Delta\ddot{q} \end{Bmatrix} + \begin{pmatrix} R_1 & R_2 \\ R_3 & R_4 \end{pmatrix}\begin{Bmatrix} \Delta\theta \\ \Delta q \end{Bmatrix} = \begin{Bmatrix} \Delta\tau \\ 0 \end{Bmatrix} \tag{19}$$

and $\Delta\tau = \tau - \tau^*$, where τ is total torque applied and τ^* is the torque holding the arm at θ^* position.

4.3 Pole Placement Method

Solving equation (19), gives

$$\begin{Bmatrix} \Delta\ddot{\theta} \\ \Delta\ddot{q} \end{Bmatrix} = \bar{\mathbf{A}}\begin{Bmatrix} \Delta\theta \\ \Delta q \end{Bmatrix} + \bar{\mathbf{B}}\,\Delta\tau \tag{20}$$

where

$$\bar{\mathbf{A}} = -\begin{pmatrix} M_1^* & M_2^* \\ M_3^* & M_4^* \end{pmatrix}^{-1}\begin{pmatrix} R_1 & R_2 \\ R_3 & R_4 \end{pmatrix}, \quad \bar{\mathbf{B}} = \begin{pmatrix} M_1^* & M_2^* \\ M_3^* & M_4^* \end{pmatrix}^{-1}\begin{Bmatrix} 1 \\ 0 \end{Bmatrix}$$

equation (20) can be written in a state space form given by

$$\dot{\mathbf{x}} = \mathbf{A}\mathbf{x} + \mathbf{B}\,\Delta\tau \tag{21}$$

where

$$\mathbf{x} = [\Delta\theta\ \Delta q\ \Delta\dot{\theta}\ \Delta\dot{q}]^T$$

$$\mathbf{A} = \begin{pmatrix} \mathbf{0} & \mathbf{I}_{2\times 2} \\ \bar{\mathbf{A}} & \mathbf{0} \end{pmatrix}, \quad \mathbf{B} = \begin{Bmatrix} \mathbf{0} \\ \bar{\mathbf{B}} \end{Bmatrix}, \quad \mathbf{I}_{2\times 2} = \begin{pmatrix} 1 & 0 \\ 0 & 1 \end{pmatrix}$$

If we choose the control law of the form

$$\Delta\tau = -\mathbf{K}\mathbf{x} = -[k_1 k_2 k_3 k_4]\mathbf{x}$$

then equation (21) becomes,

$$\dot{\mathbf{x}} = (\mathbf{A} - \mathbf{B}[k_1 k_2 k_3 k_4])\mathbf{x} \tag{22}$$

The poles of the feedback system described by equation (22) can be placed arbitrarily by choosing suitable values of the state feedback gain vector **K**. However, the feedback gain vector **K** should be chosen carefully so as not to exceed the allowable input torque.

The system without stabilizer has two poles in the left-hand side of s-plane and the other are on the imaginary axis if we neglect small structural damping. A reasonable choice of new pole locations including the stabilizer is to keep the stable pole associated with joint PD controller where they are, and move the elastic poles on the imaginary axis to the left-hand side of the s plane so that the complete system is stable.

From equation (4), we know that the stable poles in the z-plane are $z_1, z_2 = 0.95 \pm 0.035j$. With a sampling period of $T = 0.01$ sec, the pole locations in s plane become

$$S_{12} = -5.13 \pm 3.68j \tag{23}$$

Without the stabilizer, the other two poles which are on the imaginary axis can be calculated from equation (21). Table I shows the values of poles on the imaginary axis for different arm configurations. The new pole locations for the stabilizer consists of the poles of a joint controller (equation 23) and the poles shifted to the left from the imaginary axis. Table II shows the value of the gain vector **K** for various pole locations.

As shown in Table II, there is a little change in the magnitude of state feedback gains, **K**. However, the gain

Table I. Location of poles for various arm positions

Arm position	Pole location
0° (horizontal position)	$\pm 159j$
25°	$\pm 162.5j$
50°	$\pm 165.3j$
75°	$\pm 167.7j$

Table II. Feedback gain vector **K** for various pole locations

Pole location	State feedback gain **K**
$-2 \pm 165.3j$	[0.155 68.39 0.0065 −0.029]
$-2 \pm 2j$	[0.146 68.42 0.0049 −0.030]
$-10 \pm 2j$	[0.220 67.85 0.0250 −0.048]

Table III. The value of **K** for various arm positions

Arm position	State feedback gain **K**
10°	[0.0912 65.136 0.00346 −0.0326]
20°	[0.1110 66.074 0.00387 −0.0321]
30°	[0.126 66.984 0.00427 −0.0316]
40°	[0.138 67.731 0.0046 −0.0311]
50°	[0.146 68.427 0.0050 −0.0307]
60°	[0.151 68.911 0.0051 −0.0304]

changes drastically if the real part of the poles becomes less than -50, which causes an actuator torque saturation. In our experiment, the poles of $(-5.13 \pm 3.68j)$ and $(-2 \pm 2j)$ are assigned to the system of equation (22). Table III shows the value of **K** of the stabilizer for different arm positions.

It should be pointed out that the feedback gains shown in Table II and III have been obtained for the stability of equation (22). Since the feedback gains k_p and k_d have been already used in the PD controller, and a power amplifier is present in the loop, the gain vector required in the stabilizer needs to be modified. Furthermore, these gains only guarantee stability. In order to obtain good performance, these stabilizer gains were adjusted by observing the experimental results.

5. CONTROLLER IMPLEMENTATION

Since the velocity feedback signal from motor is directly fed to the amplifier, the realization of a joint controller is nothing more than implementing the following difference equation:

$$\begin{aligned} v_n &= k_p e_n \\ e_n &= x_n - \theta_n + x_n f(1 - z^{-1}) \end{aligned} \tag{24}$$

Hence v_n is the signal input to the amplifier and k_p is the proportional gain. The x_n is a command signal, and the feedforward gain f and the proportional gain k_p were set to $k_p = 0.8$ and $f = 7.6$.

As discussed previously, the vibration stabilizer can be realized by the control law

$$\begin{aligned} \Delta\tau &= -[k_1 k_2 k_3 k_4]\mathbf{x} \\ \mathbf{x} &= [\Delta\theta \ \Delta q \ \Delta\dot{\theta} \ \Delta\dot{q}] \end{aligned} \tag{25}$$

The $\Delta\tau$ is an actuation torque needed to suppress the arm vibration which is superimposed on the joint torque τ. The values of $\Delta\theta$ and q are obtained using the encoder and deflection sensor, respectively. The value of q^* is obtained by on-line calibration at the initial arm position. Since $\Delta\dot{\theta} = \dot{\theta}$ and $\Delta\dot{q} = \dot{q}$, $\Delta\dot{\theta}$ is obtained by using the tachometer output with A/D converter and $\Delta\dot{q}$ is calculated on-line by differentiating a q. For on-line differentiation, a second order backward difference equation is used

$$\Delta\dot{q}_n = \dot{q}_n = \frac{3q_n - 4q_{n-1} + q_{n-2}}{2T} \tag{26}$$

where T = sampling time, 0.01 sec

Figure 9 shows the block diagram of an overall system implemented for the flexible robotic arm.

6. EXPERIMENTAL RESULTS

6.1 Arm control: Nominal payload

The experiment was done to maneuver the arm from $\theta(0) = 0°$ to $\theta^* = 60°$ and then was brought back to $\theta^* = 0°$. The chosen command trajectory was the same as that of Fig. 7. The stabilizer was switched only for $t \in [t_{c1}, t_{02}]$ and $t \geq t_{c2}$ when the trajectory researched the vicinity of the terminal state. For the chosen command input the stabilizer is closed only during the interval $[t_{c1}, t_{02}]$ and for $t \geq t_{c2}$. The result of the experiment is presented in Figure 10(a) and (b) for the comparison of the deflection of the arm with and without stabilizer. When the stabilizer loop is open, we observe bounded oscillation (Figure 10(a)). Figure 10(b) clearly show a damping of the elastic mode.

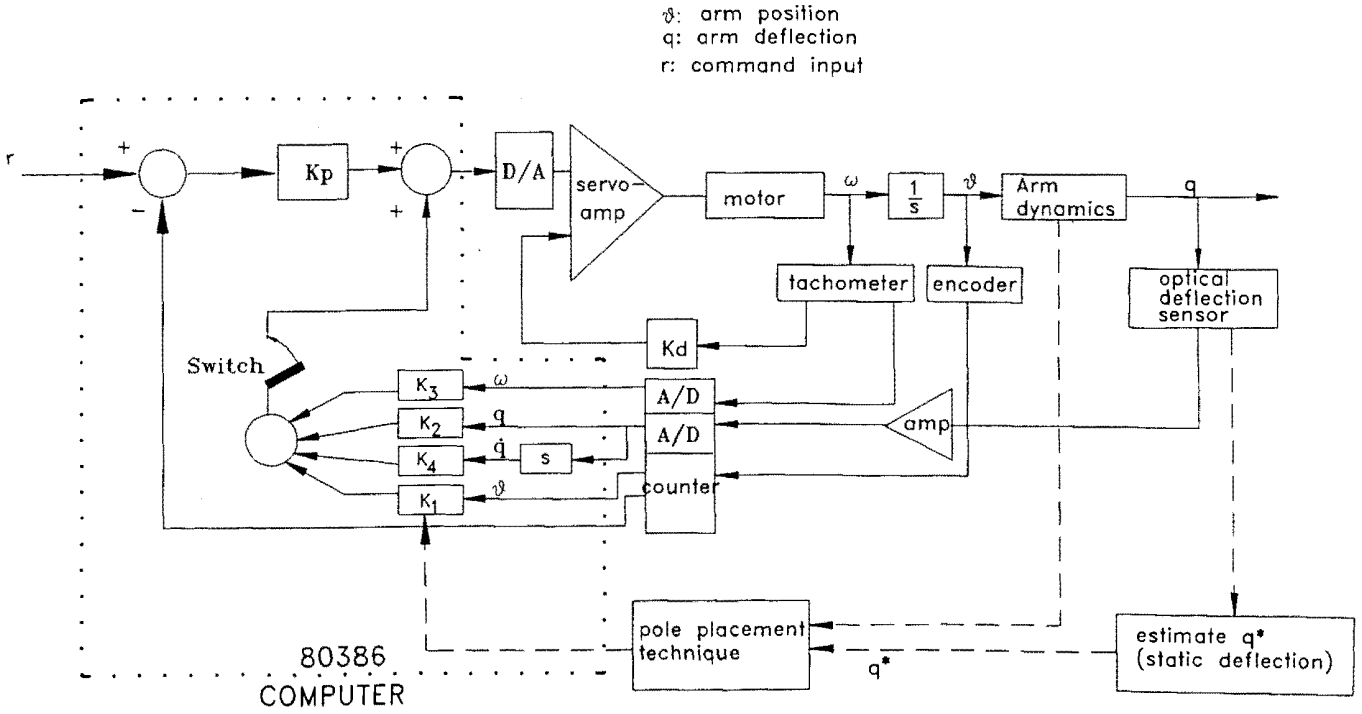

Fig. 9. Block diagram of overall control system.

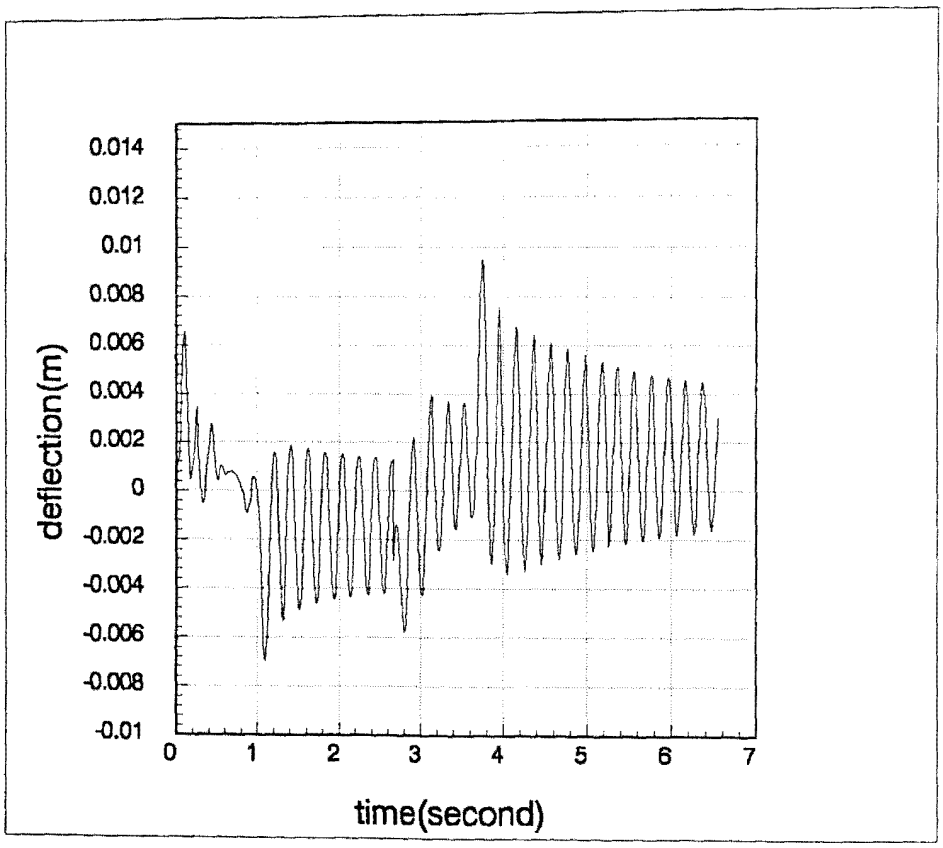

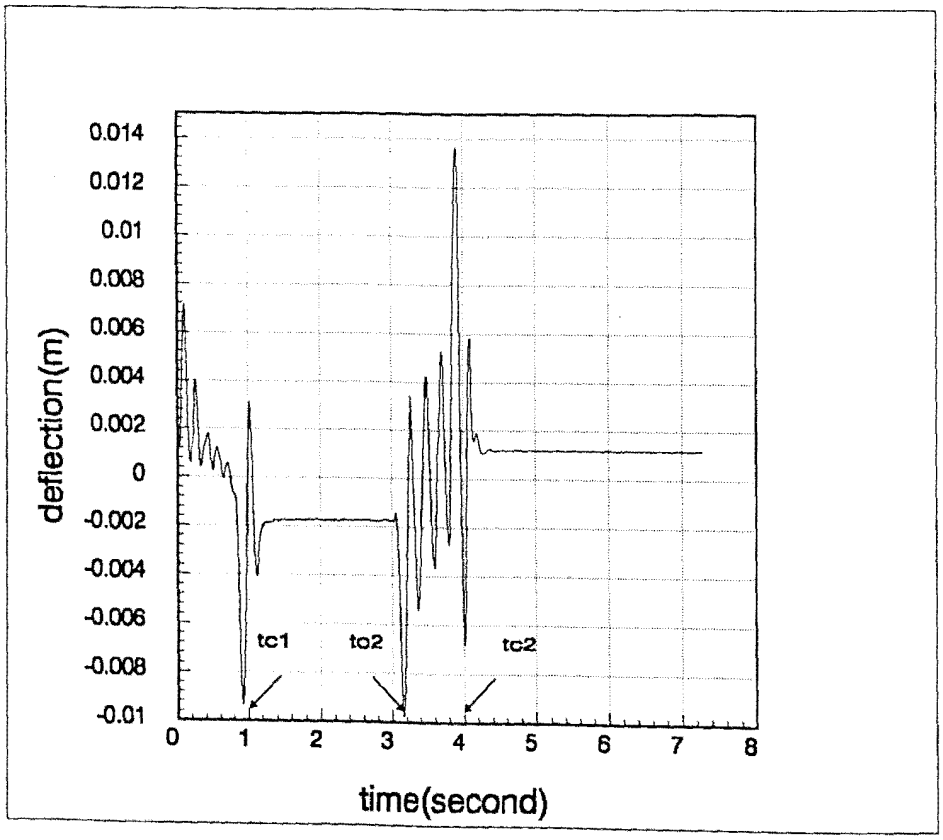

Fig. 10. (a) Plot of link deflection without stabilizer; (b) Plot of link deflection with stabilizer loop closed.

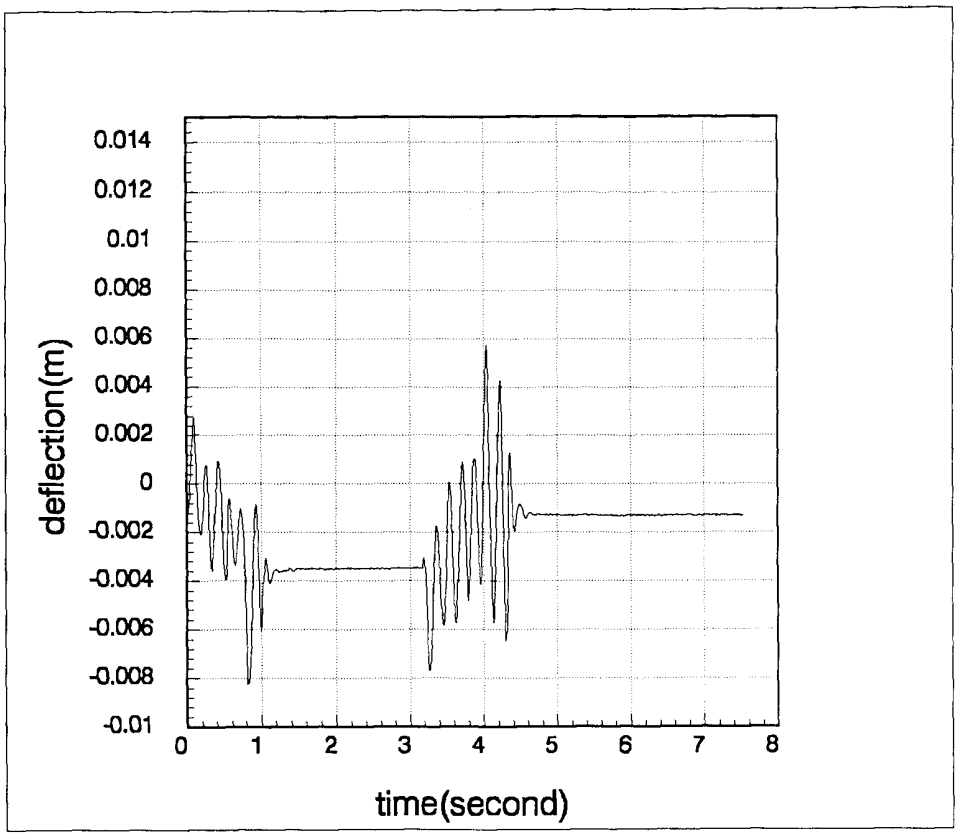

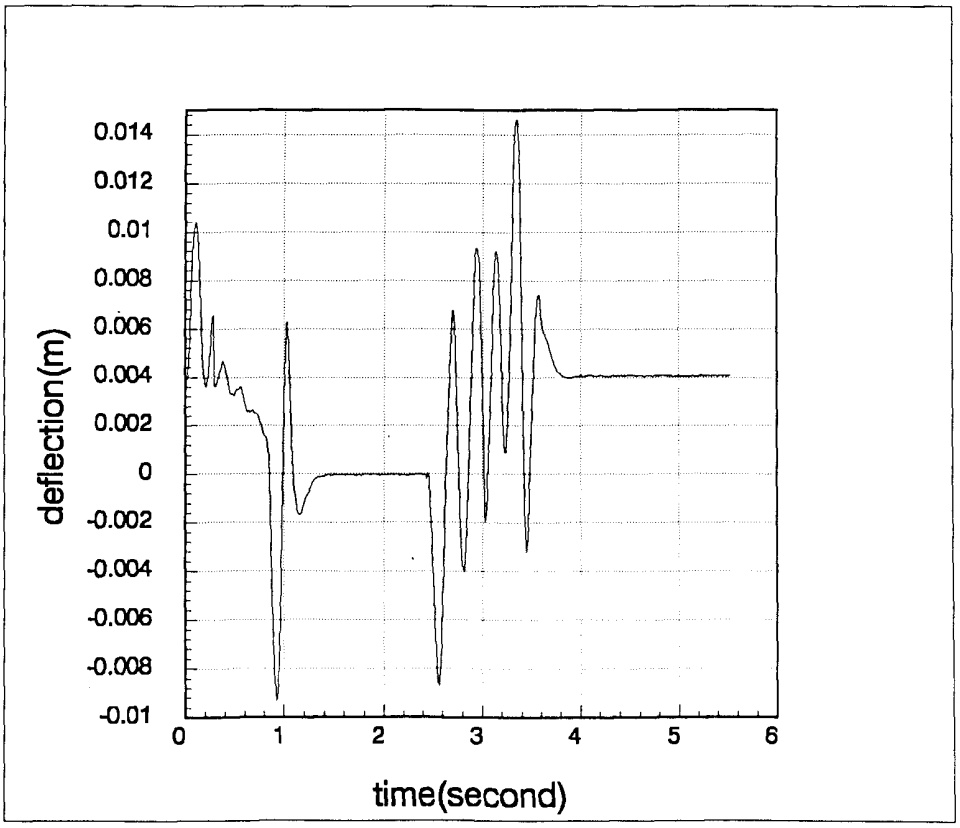

Fig. 11. (a) Plot of link deflection with $m = 0.372$ kg; (b) Plot of link deflection with $m = 1.1$ kg.

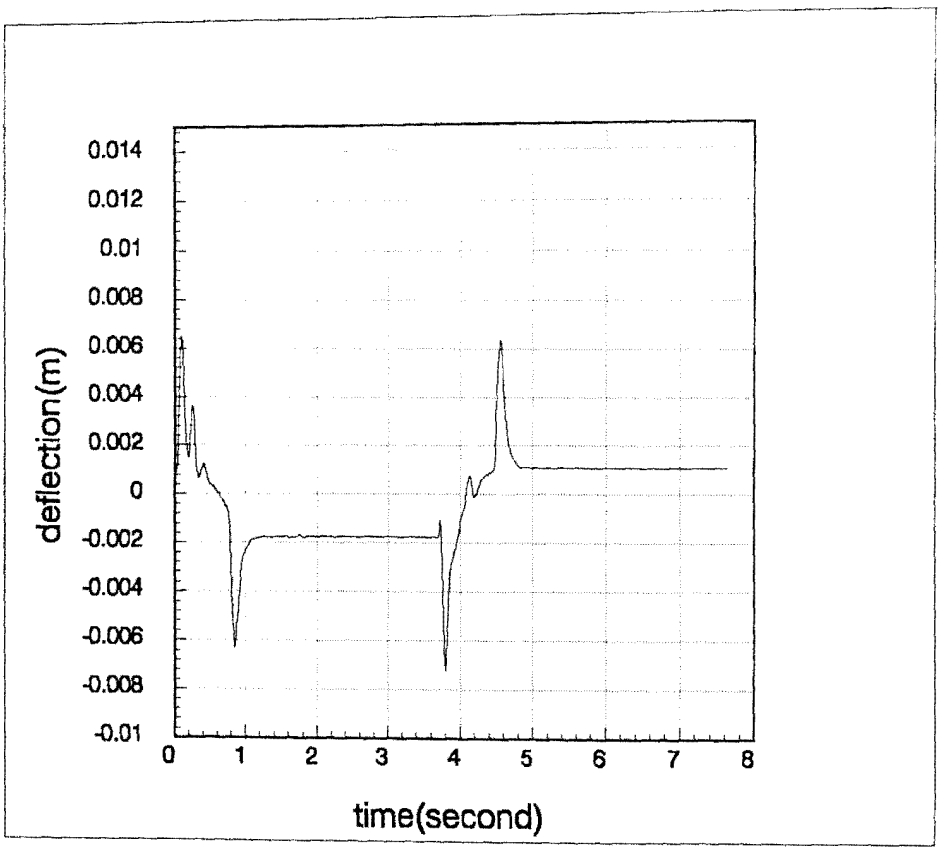

Fig. 12. Link deflection with trajectory vibration control with a ramp command trajectory.

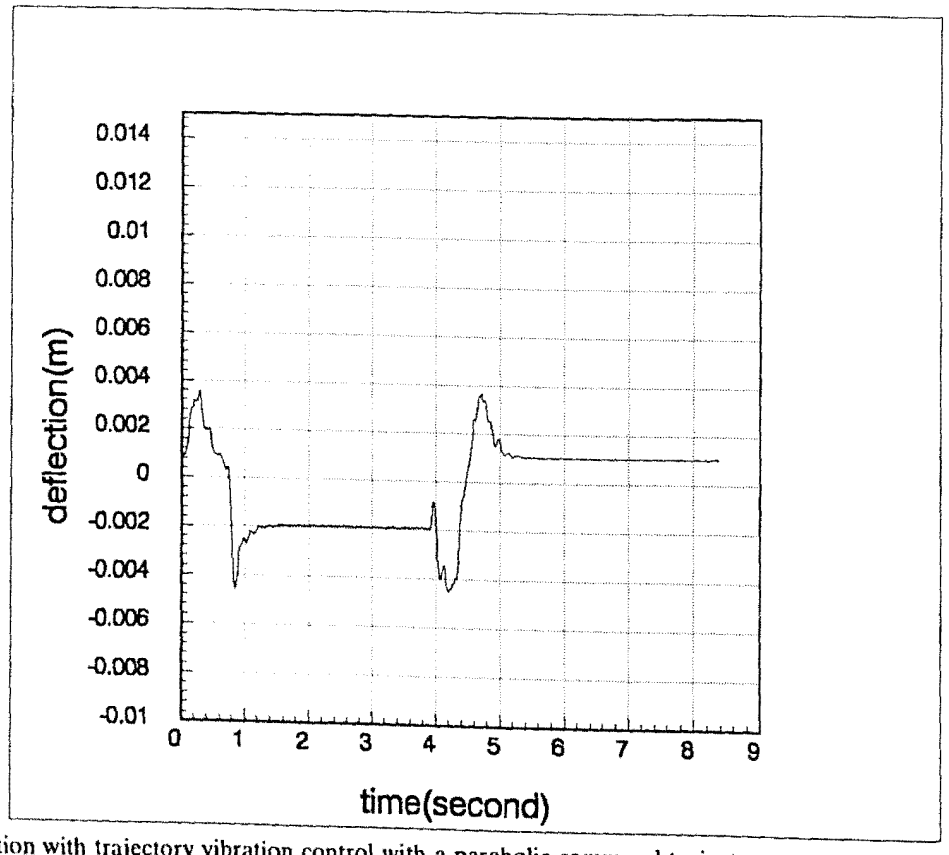

Fig. 13. Link deflection with trajectory vibration control with a parabolic command trajectory.

6.2 Arm control: Payload sensitivity

An experiment was done to examine the sensitivity of the controller to payload variations. The controller designed for the nominal payload was retained and an estimate of new q^*, i.e. static deflection at the final target position, was obtained from the deflection sensor mounted on the tip before the arm was maneuvered. Figure 11(a) and (b) show the effect of link tip load variation on the link deflection using the vibration controller designed for $m = 0.728$ kg. Two different masses of 0.372 kg and 1.1 kg are used. In this experiment, the value of q^* is updated for a given link tip load using the deflection sensor to calculate the correct value of Δq. The joint angle control and the damping of vibration are observed in each case.

6.3 Arm control: Effect of switching instant of stabilizer and smoother command trajectory

In the cases of Section 6.1 and 6.2, the stabilizer-loop was closed only over certain intervals of time. Experiments were done by keeping the stabilizer-loop closed all the time. In this case the vibration suppresion was found to be relatively better than the previous case, as shown in Figure 12.

It is seen that at those instants where the reference trajectory has corners (see Figure 7) larger elastic oscillations occur. It is expected that these peaks in oscillations can be reduced, if the command trajectory is smoother than the one used in Figure 12. In order to examine this, a smoother parabolic command trajectory[12] was used in the experiment. As shown in Figure 13, a smoother joint angle command trajectory improves vibration damping as expected.

7. CONCLUSION

The paper presents a control system design and experimental results for a one-link flexible robotic arm. In the closed-loop system, a PD controller, a feedforward filter, and a linear stabilizer were included for joint angle trajectory tracking and damping of the structural vibration of the flexible arm. The feedforward filter was designed for input shaping so that a ramp joint angle command trajectory can be followed. The optical deflection sensor was used for the synthesis of the vibration stabilizer and for the on-line prediction of the static deflection (q^*) of the arm for an unknown payload at the tip. The experimental results showed that with the dual-mode control system, accurate joint angle tracking and elastic mode stabilization can be accomplished.

Acknowledgement

This research was supported by the U.S. Army Research Office, U.S. ARO grant DAAL-03087-G-0004.

References

1. K.H. Low, "A Systematic Formulation of Dynamic Equation for Robot Manipulator with Elastic Links" *J. Robotic System* **4** No. 3, 435–456 (1987).
2. W.J. Book, "Recursive Lagrangian Dynamics of Flexible Manipulator" *Int. J. Robotic Research* **3,** 87–101 (1984).
3. M. Trabia and W. Yim, "Dynamics simulation of a three degree of freedom hydraulically activated robotic arm with flexible links." *SME Transactions on Robotics Research* **1,** 8–17 to 37 (1990).
4. T.C. Yang, K.H. Sung, J. Yang and P. Kudva, "An Experimental Adaptive Control Scheme for a Flexible Manipulator" *Int. J. Robotics and Automation* **3,** No. 2, 79–85 1988).
5. Y.P. Yang and J.S. Gibson, "Adaptive control of a manipulator with a flexible link" *Technical Report ICASE Report No.* 88-17, *ICASE, NASA Langley Research Center,* 1988 (NASA Contractor Report 181637).
6. D.M. Rovner and R.H. Cannon Jr., "Experiments Toward On-Line Identification and Control of a Very Flexible One-Link Manipulator" *Int. J. Robotics Research* **6,** No.4, 3–19 (Winter 1987).
7. S.N. Singh and A.A. Schy, "Control of Elastic Robotic Systems by Nonlinear Inversion and Modal Damping", *ASME Transactions, J Dynamic Systems, Measurement, and Control* 180–189 (Sept., 1986).
8. A. Das and S.N. Singh, "Nonlinear Adaptive Control and Linear Stabilization of an Elastic Arm," *Int. J. Robotics and Automation* **5,** No.3, 115–123 (1990).
9. W. Yim, "End-point deflection and slope measurement of a flexible robot arm" *Proc. of the SPIE's 33rd Annual International Technical Symposium on Optical and Optoelectronic Applied Science & Engineering,* Aug., 1989, San Diego, California **1167,** 194–203 (1989).
10. J.G. Bollinger and N.A. Duffie, *Computer Control of Machines and Processes* (Addison-Wesley Publishing Co., USA, 1988).
11. L. Meirovitch, *Analytical Methods in Vibration* (The MacMillan Co., New York, 1967).
12. J.J. Craig, *Introduction to Robotics* (Addison-Wesley Publishing Co., 2nd ed., USA, 1989).